

**Yang Yang**  
 Department of Mechanical and  
 Automation Engineering,  
 The Chinese University of Hong Kong,  
 Hong Kong, China  
 e-mail: [cuhkyang@gmail.com](mailto:cuhkyang@gmail.com)

**Keyu Chen**  
 Department of Mechanical and  
 Automation Engineering,  
 The Chinese University of Hong Kong,  
 Hong Kong, China  
 e-mail: [chenkeyu\\_hk@163.com](mailto:chenkeyu_hk@163.com)

**Ping Guo<sup>1</sup>**  
 Mem. ASME  
 Department of Mechanical Engineering,  
 Northwestern University,  
 Evanston, IL 60201  
 e-mail: [ping.guo@northwestern.edu](mailto:ping.guo@northwestern.edu)

# Noncontact Planar Stage Based on Near-Field Acoustic Transportation

*Acoustic radiation force in the near-field of a vibrating source can be utilized to lift and transport objects, which provides a noncontact driving technology in addition to maglev. This paper presents a novel design of a self-levitated planar stage based on near-field acoustic transportation. A closed-loop system is proposed to design a capacitance surface encoder to provide direct two-dimensional (2D) position feedback. A dynamic model based on the Reynolds equation is established to study its driving mechanism. A prototype including the levitation stage, encoder, and controller is implemented to demonstrate the potential of arbitrary trajectory tracking in two-dimensional space.*

[DOI: 10.1115/1.4046693]

*Keywords:* near-field acoustics, encoder, planar stage, vibration

## Introduction

Noncontact actuators have been favored for their low wear, low friction, zero backlash, higher operation speed, and higher efficiency, compared with conventional mechanical bearings. They have found wide applications in ultraprecision machines, semiconductor manufacturing systems, and scanning probe microscopes. Conventionally, noncontact motors based on magnetic levitation [1] and air bearings [2] have been widely used and commercialized. However, maglev and air bearing-based levitation still suffer from many practical issues, such as high costs, complicated system designs, limited motion range, electromagnetic interference, undesirable operation noises, etc.

Alternatively, acoustic levitation can be used to suspend objects without an external supply of pressurized air as opposed to air bearings. Acoustic levitation has been initially used to levitate small objects near the pressure nodes of an acoustic standing wave which are formed between an ultrasonically vibrating source and a reflector [3] or holographic acoustic elements [4]. When the levitated object serves as a reflector and reaches a near field of the vibrating source, the levitation force grows nonlinearly with the decrease in the air film thickness. This phenomenon is coined as the near-field acoustic levitation and brings the potential to use acoustic radiation force for lifting and even transporting heavy objects [5]. It can be explained by the squeeze film effect or from the fact that the viscous medium cannot be squeezed out from the thin gap instantaneously giving rise to a stiffening effect.

Due to the nonlinear increase in the near-field acoustic radiation force, heavy objects can be levitated using a circular vibrating plate [6]. If a traveling wave is introduced to the vibration plate, a directional viscous force of air will drive the levitated object to move in the direction of wave propagation to achieve noncontact transportation. Conventionally, the guide rail was excited using its flexural vibration to generate a traveling wave for one-dimensional motion [7]. Alternatively, the levitated object itself can be excited to generate vibratory motion, so a self-sustained thin air film can be created beneath the object to achieve self-levitation over a stationary ground substrate. A pseudo-traveling

wave can be further added to the object vibration to introduce similar acoustic streaming for lateral driving [8].

In order to develop the nonfield acoustic transportation technology into a noncontact positioning stage, a proper encoder is imperative for multi-degrees-of-freedom (DOF) position feedback. Few metrology or encoder systems have been developed for the measurement of planar motion of a surface actuator, not to mention 6DOF motion. Two-dimensional (2D) surface encoders based on capacitive sensors [9], optical encoders, and inductive sensors [10] have been demonstrated to measure planar motion, but cannot handle the in-plane rotation of the actuator. Gao et al. [11] utilized angle grids to provide up to five axis motion measurements. More recently, Lu and Rao [12] developed a stereo camera-based position measurement system that can provide position feedback in 6DOFs for a maglev stage.

This paper presents a novel design of a self-levitated planar stage based on near-field acoustic transportation. A closed-loop system is proposed to design a capacitance surface encoder to provide direct two-dimensional position feedback. A dynamic model based on the Reynolds equation is established to study its driving mechanism. A prototype including the levitation stage, encoder, and controller is implemented to demonstrate the potential of arbitrary trajectory tracking in two-dimensional space.

## Operation Principle and Dynamic Modeling

We have previously proposed a new driving mechanism based on near-field acoustic levitation to achieve two-dimensional noncontact motion [13]. Compared with the conventional designs based on near-field acoustic levitation, the proposed design is unique in a way that: (1) it utilizes the acoustic radiation force not only for levitation but also for transverse motion; (2) it eliminates any external component (guide rails, magnets, and air supplies), but requires only a smooth surface to operate; and (3) it has two-dimensional motion capability with higher load capacity and efficiency.

The proposed design exploits near-field acoustic levitation for self-levitation and coupled resonant vibration to generate unbalanced acoustic force in designated directions. The principle of operation is illustrated in Fig. 1, where the structure has a longitudinal as well as a bending mode. It is carefully designed such that the resonant frequencies of the two modes, namely the first longitudinal and the second bending modes, are identical. The superposition of the two normal modes results in the elliptical vibration of

<sup>1</sup>Corresponding author.

Contributed by the Manufacturing Engineering Division of ASME for publication in the JOURNAL OF MICRO- AND NANO-MANUFACTURING. Manuscript received October 23, 2019; final manuscript received March 12, 2020; published online April 1, 2020. Assoc. Editor: Lawrence Kulinsky.

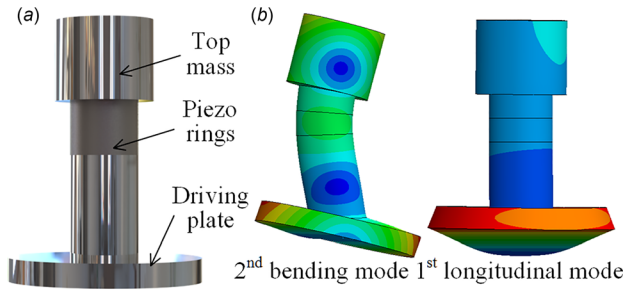


Fig. 1 (a) Design and (b) resonant modes of the design

the structure to provide the vertical levitation force as well as the propulsion force in the tilt direction of the elliptical trajectory. The piezo-electric rings, which are sandwiched between the top mass block and the bottom driving plate, have four isolated quarter-circle electrodes that can be energized individually. By adjusting the relative phase between the excitation signals to the four quadrants, one can control the moving direction and velocity in the  $XY$  plane.

In order to study the levitation and driving mechanisms of the proposed design, a simplified two-dimensional analytical model is established as shown in Fig. 2. The driving plate is modeled as a rigid plate of length,  $L$ , which is vibrating both in the vertical direction due to the longitudinal mode and around its center axis (angle  $\phi$ ) due to the bending mode. These two harmonic excitations have a phase angle,  $\delta$ , which corresponds to the relative phase between the two excitation signals.

The nominal air film thickness is set at  $100\ \mu\text{m}$ . The actual air gap distribution,  $h(x, t)$ , will vary according to the plate vibration motion. The time-varying pressure distribution,  $p(x, t)$ , within the air film can be modeled using the modified Reynolds equation [14]

$$\frac{\partial [p(x, t)h(x, t)]}{\partial t} = \frac{\partial}{\partial x} \left[ \frac{h(x, t)^3 p(x, t)}{12\mu} \frac{\partial p(x, t)}{\partial x} \right] \quad (1)$$

where  $\mu$  is the air viscosity.

Certain assumptions are made for the application of the Reynolds equation that (1) air is assumed to be a Newtonian compressible fluid; (2) the air gap thickness (film thickness) is much smaller than the vibrating plate geometry; and (3) the variation of pressure across the film thickness is negligible. Air pressure distribution is calculated by solving Eq. (1) subject to the initial and boundary conditions of an atmospheric pressure outside the air film region. There are two forces acting on the bottom surface of the driving plate, namely the acoustic radiation pressure acting perpendicular to the driving plate and the viscous force due to the air velocity gradient parallel to the driving plate. Considering the fact that the

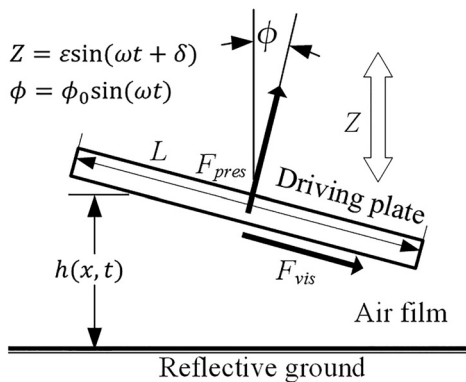


Fig. 2 Schematic of the dynamic model

tilting angle,  $\phi$ , is very small, and the acoustic pressure is much larger than the viscous stress, the levitation force can be derived by integrating the pressure over the driving plate area and take the average result over a cycle, as

$$F_{\text{levi}} = \frac{1}{T} \int_0^T \int_0^L A(p - p_0) dx dt \quad (2)$$

The transverse driving force is composed of the lateral component of the acoustic pressure and the viscous force due to the pressure gradient. If we assume that the boundary conditions are fixed to zero at the ground for flow velocity, and set as the transverse velocity of the driving plate at the top, the shear stress at the driving plate can be calculated as

$$\tau_{\text{vis}}(x, t) = \frac{h(x, t)}{2} \frac{\partial p(x, t)}{\partial x} \quad (3)$$

The driving force then can be derived considering the tilting angle, which is given by

$$F_{\text{drv}} = \frac{1}{T} \int_0^T \int_0^L A \left[ (p - p_0) \sin \phi(x, t) + \frac{h}{2} \frac{\partial p}{\partial x} \right] dx dt \quad (4)$$

Three representative cases have been calculated corresponding to the pure longitudinal, pure bending, and combined longitudinal and bending vibration. The spatial distribution ( $X$ -axis) of pressure and air film thickness as well as their time evolution ( $Y$ -axis) are plotted in Fig. 3. The pressure is normalized as the ratio over the atmospheric pressure. The air film thickness is plotted as the deviation from the nominal air gap. For the pure longitudinal vibration case, the air film thickness is constant along the driving plate at any time instance, but varying with time. The maximal pressure is larger than the minimal pressure due to the squeeze film effect, which provides a positive levitation force when averaged over one cycle. For the pure bending vibration case, the air film thickness is symmetric both with respect to location and time. The levitation force, however, is smaller than that for the pure longitudinal vibration.

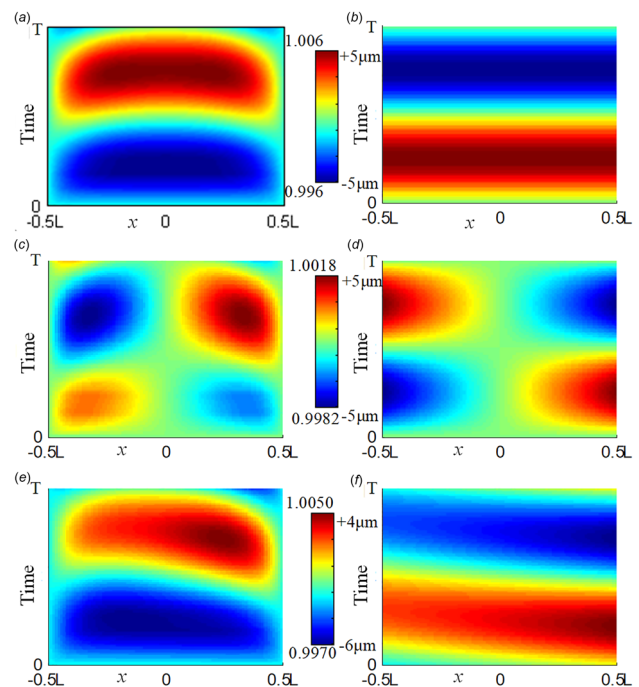


Fig. 3 Pressure and air film thickness distribution for (a and b) longitudinal, (c and d) bending, and (e and f) combined vibration

For the combined longitudinal and bending vibration mode, the pressure distribution is not symmetric in the spatial or time axis. The pressure gradient term then will be nonzero over one cycle, which contributes to the viscous force. However, unlike previous designs [5,7,8], the driving force contributed from the viscous term is negligible. In fact, the viscous force is much smaller (more than one order of magnitude) than the lateral component of acoustic pressure. The tilting angle,  $\varphi$ , is the main reason that we could get much higher energy efficiency and a larger driving force using this coupled resonant structure design. Since the tilting angle flips its sign between the air compression and expansion phases, the  $p-p_0$  and  $\sin\varphi$  terms will always have the same sign in Eq. (4). The instantaneous driving force will then always point to the designated direction over the whole period. Though the proposed model takes simplified 2D vibration motion of the plate, the calculated forces are quite comparable to our previous experimental results [13]. For this particular combined vibration case, the calculated driving force is 9.2 mN, while the viscous force is only  $1.56 \times 10^{-4}$  mN. If we assume a linear relationship between the input phase angle,  $\delta$ , and the vibration amplitude ratio of the two modes, the relationship between the driving force and the input phase difference is established accordingly, as shown in Fig. 4. The driving force is scaled regarding the levitation force (which equals to the stage weight) and normalized to unity.

### Capacitance Encoder Design and Calibration

A planar encoder is proposed to provide position feedback signals to our stage. The encoder design is based on the measurement of capacitance change between the driving stage and the metal sensing plates embedded in the ground. Due to the stage levitation, the ground sensing plates, driving plate, and thin air film form a capacitor. Its capacitance is proportional to the overlapping area between the circular stage and the sensing plate; and inversely proportional to the thickness of the air film. As illustrated in Fig. 5, the metal sensing plates are equally divided into four isolated square sensing segments, which are partially covered by the circular stage. The measured capacitances are correspondingly labeled as  $C_1$ - $C_4$ . The lateral position (in the XY plane) of the

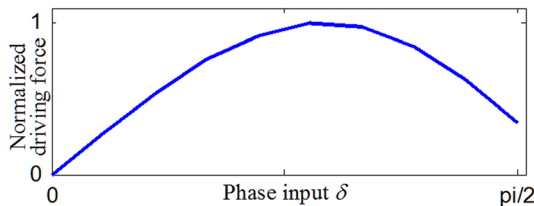


Fig. 4 Relationship between the driving force and the input phase angle

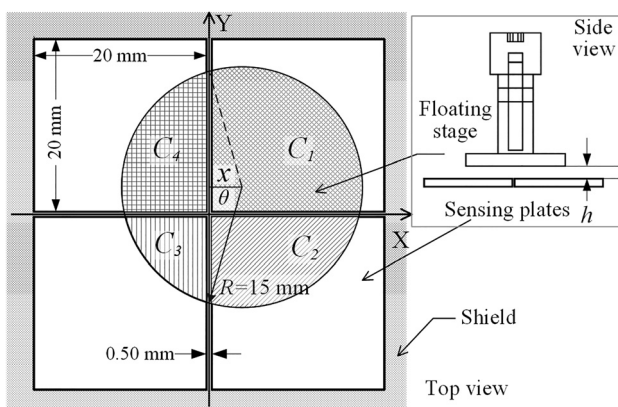


Fig. 5 Configuration of the capacitance surface encoder

circular stage can be uniquely determined based on the capacitance values.

For example, the calculation of X coordinates is explained as follows. The capacitance of the right- and left-side sensing segments are determined by the geometric relationship as

$$C_1 + C_2 = \frac{\varepsilon}{h}(A_1 + A_2) = \frac{\varepsilon}{h} \left[ R^2(\pi - \theta) + \frac{R^2 \sin 2\theta}{2} \right] \quad (5)$$

$$C_3 + C_4 = \frac{\varepsilon}{h}(A_3 + A_4) = \frac{\varepsilon}{h} \left[ R^2\theta - \frac{R^2 \sin 2\theta}{2} \right] \quad (6)$$

where  $\varepsilon$  is the permittivity;  $h$  is the air film thickness;  $R$  is the radius of the circular stage; and  $\theta$  is the central angle between the radii parallel to the X-axis and intersecting the Y-axis. The X coordinate is determined by the cosine value of this central angle, which is described by  $x = R \cos \theta$ .

The influence of the air film thickness on the coordinate values can be eliminated by calculating the ratio of the capacitance difference between the left and right segments to the total capacitance as

$$\alpha = \frac{C_1 + C_2 - C_3 - C_4}{C_1 + C_2 + C_3 + C_4} = \frac{2\theta - \pi - \sin 2\theta}{\pi} \quad (7)$$

The central angle  $\theta$  can be uniquely determined by solving this transcendental equation given any capacitance ratio  $\alpha$ . The range of  $\alpha$  is taken as  $-0.6$  to  $+0.6$ , considering the size constraints of the sensing plates as well as the circular stage. The function of  $\theta$  in terms of the ratio  $\alpha$  then can be fitted to a third-order polynomial with a root-mean-square error (RMSE) less than  $3.5 \times 10^{-4}$ , which is given by

$$\theta(\alpha) = 0.2016\alpha^3 + 0.7821\alpha + 1.571 \quad (8)$$

The Y coordinate can be calculated using the same procedure but using the capacitance difference between the upper and lower segments, or  $C_1 + C_4 - C_2 - C_3$ . The XY position calculation is independent of the air film thickness,  $h$ , which might be varied during the operation of the floating stage. This air film thickness, or the levitation height, can also be estimated by

$$h = \frac{\varepsilon \pi R^2}{C_1 + C_2 + C_3 + C_4} = \frac{K}{C_{\text{tot}}} \quad (9)$$

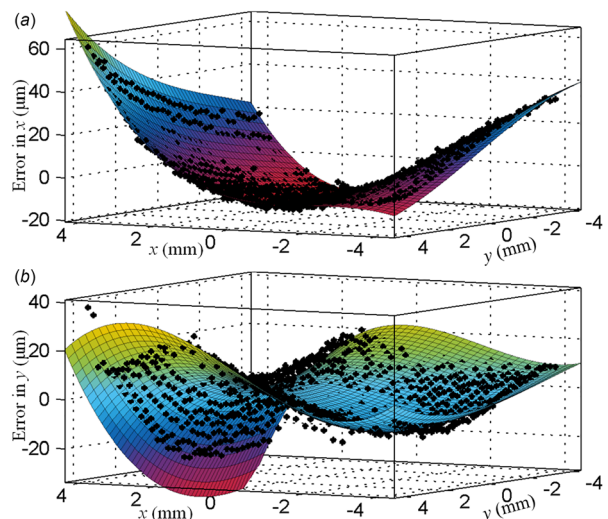


Fig. 6 Nonlinear compensation in (a) x- and (b) y-directions

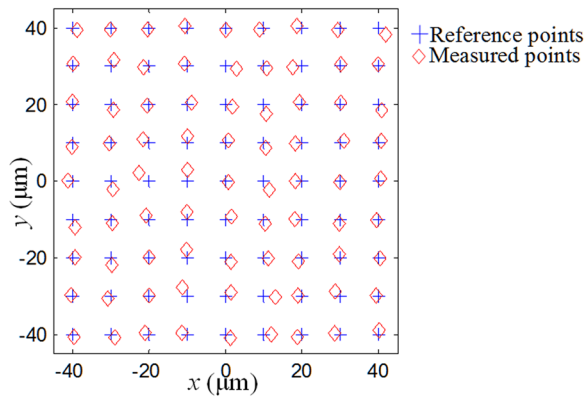


Fig. 7 Validation test results in the center area of the encoder

Table 1 Calibration of two-dimensional capacitance encoder

RMSE ( $\mu\text{m}$ )	Rotation and scaling	Nonlinear compensation
$8 \times 8$ mm (calibration)	17.3	3.6
$8 \times 8$ mm (validation)	22.0	7.1
$80 \times 80$ $\mu\text{m}$ (validation)	1.5	N/A

An encoder prototype was fabricated with a printed circuit board. The capacitance was measured using a high-resolution, four-channel capacitance-to-digital converter (FDC1004, Texas Instruments, Dallas, TX) with special considerations paid to the shielding of parasitic capacitance. The encoder was calibrated using a three-axis precision stage with nanometer resolution and uncertainty of  $\pm 250$  nm (Aerotech, Pittsburgh, PA). The coefficient  $K$  in Eq. (9) was first calibrated to be  $5307 \mu\text{m pF}$ . The  $XY$  coordinates were calibrated in an area of  $8$  mm by  $8$  mm with a grid size of  $0.25$  mm (1089 points). The air gap was kept at  $120 \mu\text{m}$ . The reference coordinates were generated from the positioning stage, while the measured coordinates were calculated based on the procedure described earlier.

The calculated coordinates were first compensated for the scaling and the misalignment of the encoder axis and the precision stage (rotation error). These errors were removed since they were not the intrinsic errors of the encoder. Then the systematic errors due to the nonlinear features were identified and fitted to a third-order polynomial equation in each axis, as shown in Fig. 6. These

nonlinear errors were suspected to be coming from the clearance distance between the sensing plates, which was ignored in our ideal model, and the roundness error of the driving plate. It should be noted that variation of stage levitation height has a negligible effect on the  $XY$  coordinate measurement, since the air film thickness,  $h$ , has been removed in the calculation of the capacitance ratio in Eq. (7). A validation test was performed on another set of data points (441 points) different from the calibration set in the same region with a different air film thickness ( $100 \mu\text{m}$ ). In addition, the encoder was tested at a small area in the center where the nonlinear error was negligible with the results illustrated in Fig. 7. The calibration and validation results are summarized in Table 1, where the errors are evaluated in terms of the RMSE.

## Control Scheme and Experimental Results

As shown in Fig. 8, a prototype system has been designed, built and tested, which consists of: (1) a levitation stage as the actuator; (2) a capacitance encoder as the feedback module; (3) a LABVIEW program including the capacitance-to-coordinate calculation, proportional–integral–derivative control module, and driving signal generation module; and (4) a data output card and a piezo-amplifier as the driver module. There are four channels of output, connecting to the four individual quadrants of the piezorings. The stage is driven by applying two sinusoidal signals at the coupled resonant frequency with a phase shift,  $\delta$ , between them. The driving frequency and amplitude are kept constant to maintain the levitation height, while the phase shift angle is the key control parameter as the system input.

The stage moving direction depends on the excitation signal configuration and the corresponding direction of the bending mode. This driving mechanism indicates that the stage could only move in either the  $X$  or  $Y$  direction at the same time instance. In our current implementation, an alternating stepping strategy is adopted to drive the levitation stage in the  $X$  and  $Y$  direction sequentially with microsteps as shown in Fig. 9(a). The step size is determined by the displacement error calculated between the targeted location and measured coordinates.

In addition, a sudden change of the phase shift angle and switch of the motion direction during each control cycle would cause a discontinuity in the excitation signal or an impulse shock to the system. Since the friction force and damping effect are minimal for our levitation stage, the system performance would deteriorate due to unwanted vibration associated with these periodic impulses from the control signals. During each step motion, a phase

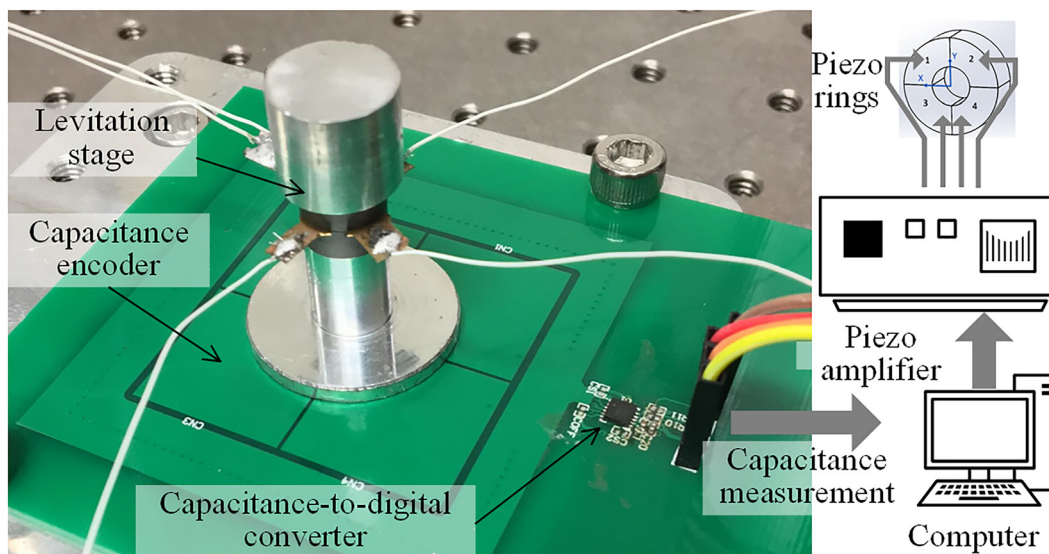
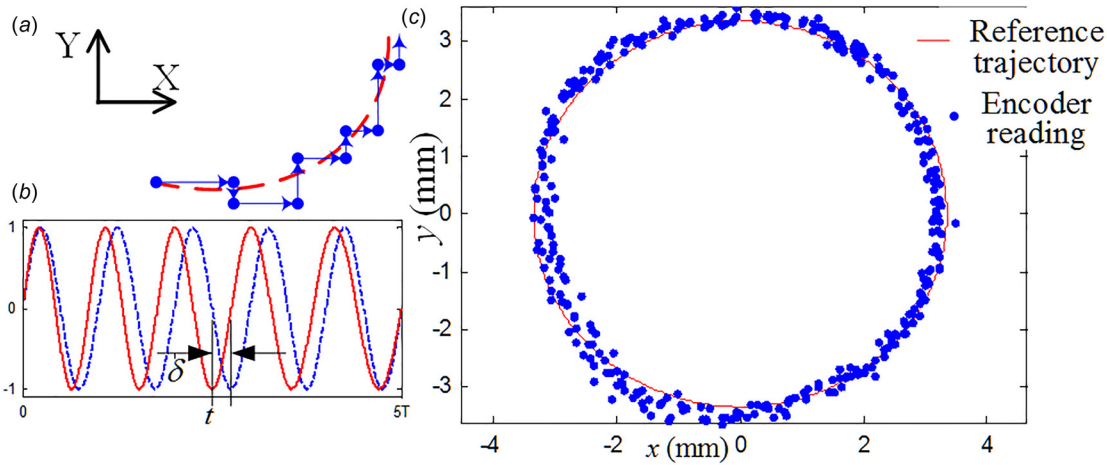


Fig. 8 Prototype design and component diagram



**Fig. 9** (a) Schematic of alternating stepping strategy, (b) phase modulation of control signals, and (c) recorded motion data of a circular trajectory

modulation technique is adopted for the smooth transition of the phase shift angle as illustrated in Fig. 9(b). The carrier signal is the ultrasonic excitation wave at the coupled resonant frequency of the device, while the message signal is a half cycle of a sine wave with an amplitude equal to the target phase difference angle,  $\delta$ . The modulation frequency determines the step motion time, which is limited by the speed of the data output card. In our current setup, it is around 30 ms.

Proportional–integral–derivative controllers are setup for each direction of motion. The controller output is compensated for the nonlinearity between the driving force and phase angle based on our dynamic model. Figure 9(c) shows the collected motion data of the stage following a circular trajectory with a radius of 3.5 mm. The errors are mainly due to the stepping motion, which is under an open-loop system during the actuation of a stepping motion. Further performance optimization will be carried out in our future work. We would also like to improve our design in the future to achieve vector motion and independent control of the levitation height to act as a 3DOF motion stage.

### Funding Data

- Northwestern University (Start-up Fund; Funder ID: 10.13039/100007059).
- Shun Hing Institute of Advanced Engineering, CUHK (RNE-p4-17; Funder ID: 10.13039/501100006355).

### References

- [1] Lu, X., and Usman, I.-U.-R., 2012, "6D Direct-Drive Technology for Planar Motion Stages," *CIRP Ann. Manuf. Technol.*, **61**(1), pp. 359–362.
- [2] Pister, K. S., Fearing, R. S., and Howe, R. T., 1990, "A Planar Air Levitated Electrostatic Actuator System," *Proceedings IEEE Proceedings on Micro Electro Mechanical Systems, An Investigation of Micro Structures, Sensors, Actuators, Machines and Robots*, Napa Valley, CA, Feb. 11–14, pp. 67–71.
- [3] Yarin, A., Pfaffenhöner, M., and Tropea, C., 1998, "On the Acoustic Levitation of Droplets," *J. Fluid Mech.*, **356**, pp. 65–91.
- [4] Marzo, A., Seah, S. A., Drinkwater, B. W., Sahoo, D. R., Long, B., and Subramanian, S., 2015, "Holographic Acoustic Elements for Manipulation of Levitated Objects," *Nat. Commun.*, **6**(1), p. 8661.
- [5] Ueha, S., Hashimoto, Y., and Koike, Y., 2000, "Non-Contact Transportation Using Near-Field Acoustic Levitation," *Ultrasonics*, **38**(1–8), pp. 26–32.
- [6] Matsuo, E., Koike, Y., Nakamura, K., Ueha, S., and Hashimoto, Y., 2000, "Holding Characteristics of Planar Objects Suspended by Near-Field Acoustic Levitation," *Ultrasonics*, **38**(1–8), pp. 60–63.
- [7] Hashimoto, Y., Koike, Y., and Ueha, S., 1998, "Transporting Objects Without Contact Using Flexural Traveling Waves," *J. Acoust. Soc. Am.*, **103**(6), pp. 3230–3233.
- [8] Koyama, D., and Nakamura, K., 2009, "Noncontact Self-Running Ultrasonically Levitated Two-Dimensional Stage Using Flexural Standing Waves," *Jpn. J. Appl. Phys.*, **48**(7), p. 07GM07.
- [9] Kolb, P., Decca, R., and Drew, H., 1998, "Capacitive Sensor for Micropositioning in Two Dimensions," *Rev. Sci. Instrum.*, **69**(1), pp. 310–312.
- [10] Hojjat, Y., Karafi, M. R., Ghanbari, M., and Lotfi, M., 2011, "Development of an Inductive Encoder for Simultaneous Measurement of Two-Dimensional Displacement," *Int. J. Adv. Manuf. Technol.*, **53**(5–8), pp. 681–688.
- [11] Gao, W., Dejima, S., Shimizu, Y., Kiyono, S., and Yoshikawa, H., 2003, "Precision Measurement of Two-Axis Positions and Tilt Motions Using a Surface Encoder," *CIRP Ann. Manuf. Technol.*, **52**(1), pp. 435–438.
- [12] Lu, X., Rao, N., and Usman, I.-U.-R., 2013, "Six-Axis Position Measurement System for Levitated Motion Stages," *CIRP Ann. Manuf. Technol.*, **62**(1), pp. 507–510.
- [13] Chen, K., Gao, S., Pan, Y., and Guo, P., 2016, "Self-Running and Self-Floating Two-Dimensional Actuator Using Near-Field Acoustic Levitation," *Appl. Phys. Lett.*, **109**(12), p. 123503.
- [14] Minikes, A., Bucher, I., and Haber, S., 2004, "Levitation Force Induced by Pressure Radiation in Gas Squeeze Films," *J. Acoust. Soc. Am.*, **116**(1), pp. 217–226.